# Shape oscillations of an oil drop rising in water: effect of surface contamination

**Nicolas Abi Chebel**[1,2,3,4], **Jiří Vejražka**[5], **Olivier Masbernat**[2,4] **and Frédéric Risso**[1,4]†

[1] Institut de Mécanique des Fluides de Toulouse, CNRS & Université de Toulouse, 31400 Toulouse, France

[2] Laboratoire de Génie Chimique, CNRS & Université de Toulouse, France

[3] IFP – Energies Nouvelles, 92852 Rueil-Malmaison CEDEX, France

[4] Fédération de Recherche FERMAT, CNRS, Toulouse, 31400 Toulouse, France

[5] Institute of Chemical Process Fundamentals, Academy of Sciences of the Czech Republic, 165 02 Prague 6-Suchdol, Czech Republic

Inertial shape oscillations of heptane drops rising in water are investigated experimentally. Diameters from 0.59 to 3.52 mm are considered, corresponding to a regime where the rising motion should not affect shape oscillations for pure immiscible fluids. The interface, however, turns out to be contaminated. The drag coefficient is considerably increased compared to that of a clean drop due to the well-known Marangoni effect resulting from a gradient of surfactant concentration generated by the fluid motion along the interface. Thanks to the decomposition of the shape into spherical harmonics, the eigenfrequencies and the damping rates of oscillation modes $n = 2$, 3, 4 and 5 have been measured. Frequencies are not affected by contamination, while damping rates are increased by a considerable amount that depends neither on drop instantaneous velocity nor on diameter. This augmentation, however, depends on the mode number: it is maximum for mode two (multiplied by 2.4) and then relaxes towards the value of a clean drop as $n$ increases. A previous similar investigation of a drop attached to a capillary has not revealed such an increase of the damping rates, indicating that the coupling between rising motion and surface contamination is responsible for this effect.

**Key words:** bubble dynamics, drops, drops and bubbles

## 1. Introduction

For low-viscosity fluids, a deformed drop generally relaxes to the spherical shape by performing damped oscillations. This dynamics involves several modes. For a drop made of pure immiscible fluids and in the absence of an external cause of motion, these modes were theoretically obtained from linearized Navier–Stokes equations (Miller & Scriven 1968; Prosperetti 1980; Lu & Apfel 1991). The geometry of each mode is given by a spherical harmonic $Y_{m,n}$ characterized by two integers, a polar wavenumber $n \geqslant 2$ and an azimuthal wavenumber $m$ satisfying $-n \leqslant m \leqslant n$. In the

† Email address for correspondence: frederic.risso@imft.fr

potential flow approximation, their frequency is given by

$$\omega_n^* = \sqrt{\frac{(n-1)n(n+1)(n+2)\sigma}{(\rho_d(n+1)+\rho_c n)a^3}}, \tag{1.1}$$

where $\rho_d$ and $\rho_c$ are respectively the density of the drop and external phases, $a$ is the drop radius and $\sigma$ is the interfacial tension. Taking vorticity into account, the frequency $\omega_n^{th}$ and damping rate $\beta_n^{th}$ of each mode are given by Lu & Apfel (1991)

$$\omega_n^{th} = \omega_n^* - \frac{\mu_c}{\rho_c a^2} B_n \sqrt{Re_{osc,n}}, \tag{1.2}$$

$$\beta_n^{th} = \frac{\mu_c}{\rho_c a^2}[C_n + B_n \sqrt{Re_{osc,n}}], \tag{1.3}$$

where $\mu_d$ and $\mu_c$ are respectively the dynamic viscosity of the drop and continuous phases, $B_n$ and $C_n$ are functions of both the density ratio $\rho_d/\rho_c$ and the viscosity ratio $\mu_d/\mu_c$, and $Re_{osc,n} = 2\rho_c\omega_n^* a^2/\mu_c$ is the oscillation Reynolds number. In (1.2)–(1.3), the terms proportional to the square root of the Reynolds number account for the role of the boundary layers that develop at the interface, while the other terms represent the contribution of the potential flow that dominates further from the interface. For a given initial shape, the problem is thus fully characterized by three dimensionless groups, $\rho_d/\rho_c$, $\mu_d/\mu_c$ and $Re_{osc} = Re_{osc,2}$.

If the drop is moving at velocity $U$ under the action of gravity, the problem involves a fourth dimensionless group, the ascending Reynolds number $Re_{asc} = 2\rho_c U a/\mu_c$. Note that the Weber number based on the rise velocity is proportional to the square of the Reynolds number ratio $Re_{asc}/Re_{osc}$, which is itself equal to the rise-to-oscillation velocity ratio $U/\omega_2 a$. Provided that $Re_{asc}$ is less than one hundred and $U/\omega_2 a$ is small compared to unity, a drop may remain almost spherical and rise along a rectilinear path. If the drop shape is disturbed, its oscillations remain described by the theory derived for a non-moving drop (Subramanyam 1969; Basaran, Scott & Byers 1989).

The dynamics of a drop rising slowly might thus seem well understood. However, a tiny amount of surface-active contaminant is known to alter it significantly. Due to the opposite effect of advection and diffusion, a gradient of the surface concentration of the adsorbed contaminants may develop along the interface, which gives birth to a Marangoni effect that stops the fluid circulation within the drop or bubble and decreases the rise velocity (Cuenot, Magnaudet & Spennato 1997). For an organic liquid in water, the rise velocity of a spherical drop is generally observed to be close to that of a rigid sphere (Hu & Kintner 1955). Despite interesting recent attempts to deal with pure systems (see Wegener, Kraume & Paschedag 2010, and references therein), no experiments have matched exactly the terminal velocity of a pure drop. The problem of surface contamination is less arduous with a gas bubble: pure rising bubbles have been observed either in ultra-purified water (Duineveld 1995) or in non-polar fluids without need of an ultrapure environment (Zenit & Magnaudet 2008).

In a previous work we have investigated the shape dynamics of a drop of heptane attached to the tip of a capillary in water (Abi Chebel, Risso & Masbernat 2011, referred as ACRM hereinafter). Even though the experiments were not carried out in an ultrapure environment, the oscillations were well described by the theory for a pure system. Considering modes 2, 3 and 4, the measured frequency was within 3 % of the theoretical prediction (1.2) and the measured damping rate was found to be 20 % larger than the theoretical value (1.3); this small discrepancy was attributed to the attachment constraint that slightly coupled the different modes.

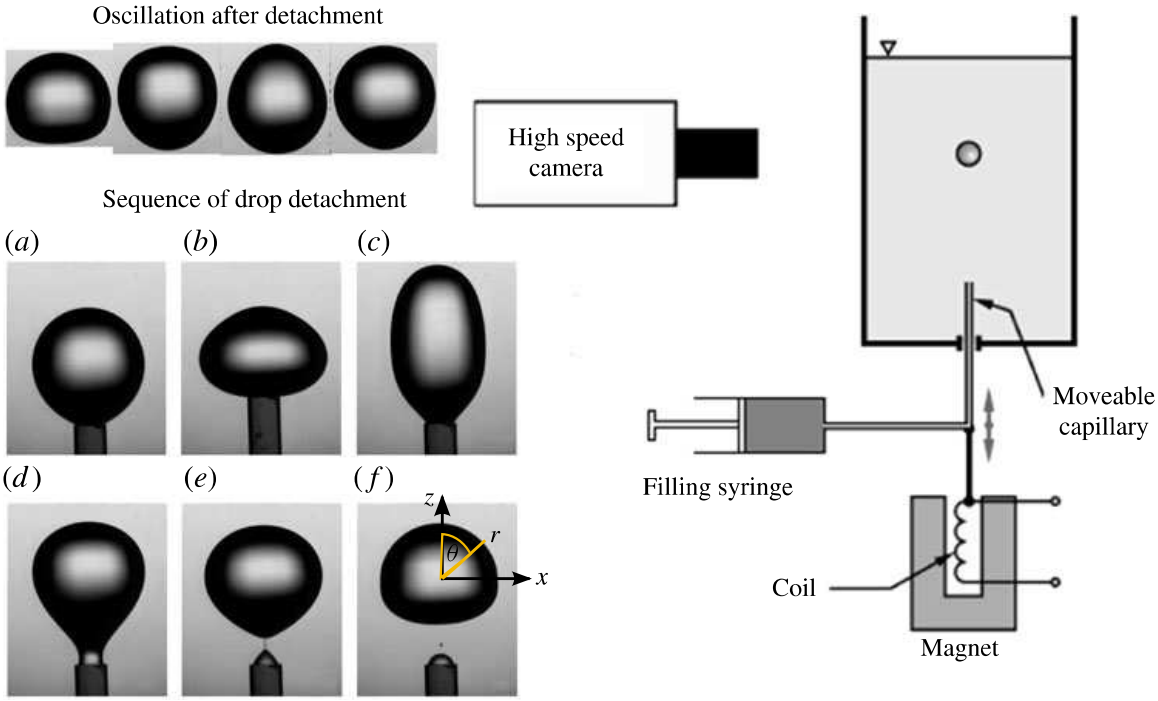


FIGURE 1. (Colour online available at journals.cambridge.org/flm) Experimental setup. Drop detachment, which occurs between images (*e*) and (*f*), is caused by the motion of the capillary tube (the images are for $d = 3.52$ mm).

In the present work, a non-spherical drop of heptane is suddenly released in still water and its damped shape oscillations are recorded and analysed as the drop is rising. The fluid system is the same as that studied in ACRM. We consider a drop size range such that the rise velocity is not expected to have any significant effect on the interface oscillations of pure fluids ($U/\omega_2 a \ll 1$). The objective is to determine whether or not the shape dynamics of a drop is altered by the Marangoni effect that develops when the drop is rising under the action of buoyancy.

## 2. Experimental setup and parameters

The experimental setup, shown in figure 1, is adapted from that of Vejražka *et al.* (2008). The external phase is distilled water ($\rho_c = 998$ kg m$^{-3}$, $\mu_c = 1.0$ mPa s$^{-1}$), further purified by activated carbon filtration and demineralization by ion exchange resin; the water is stored in an 11 cm $\times$ 11 cm $\times$ 26 cm glass vessel. The drop phase is *n*-heptane ($\rho_d = 684$ kg m$^{-3}$, $\mu_d = 0.41$ mPa s$^{-1}$) of grade p.a. with no further purification. The interfacial tension measured by a De Nouy ring tensiometer is $\sigma = 49$ mN m$^{-1}$, suggesting the presence of impurities as compared to a pure interface ($\sigma = 51$ mN m$^{-1}$); it is stored in a feeding plastic syringe (12 ml, manufacturer Braun) connected to a fused silica capillary tube of 0.25 mm inner diameter. A drop is grown up to a chosen diameter. The capillary is then rapidly moved in the vertical direction by means of an electromagnetic system, which causes both drop detachment and initial deformation. After its release, the drop starts rising under the action of buoyancy and experiences shape oscillations due to periodic exchange between surface and kinetic energy. A high-speed camera (Photron SA 1.1) equipped with a magnifying lens (Navitar 12X Zoom) is used to film the drop evolution. The image size is 324 $\times$ 864 pixels. The image resolution ranges between 13.3 and 3.64 μm and

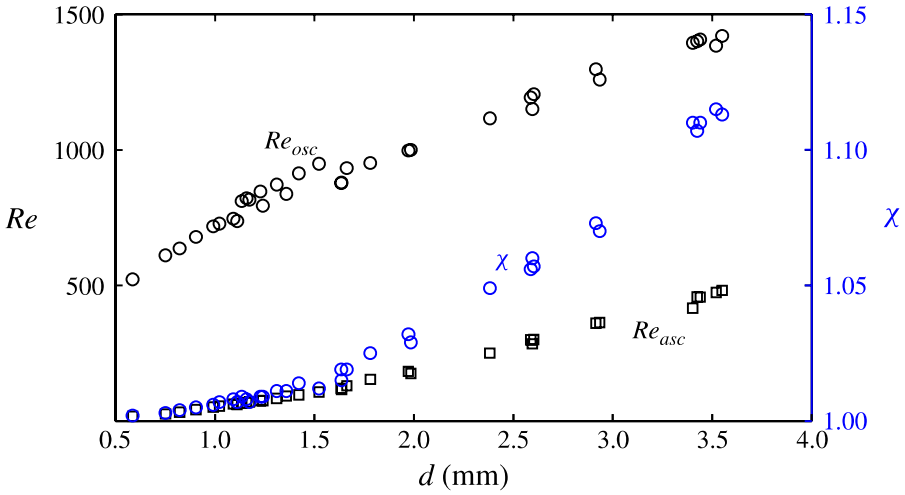


FIGURE 2. (Colour online) Drop parameters against diameter: oscillating ($Re_{osc}$) and ascending ($Re_{asc}$) Reynolds numbers; aspect ratio $\chi$.

frame rate between 10 000 and 18 000 frames $s^{-1}$, for the biggest and smallest drops respectively. Image processing is similar to that used in ACRM. The drop contour is first determined by a home-made algorithm with sub-pixel interpolation based on greyscale thresholding, leading to an accuracy of $\pm 0.4$ pixel. The drop centre and aspect ratio $\chi$ are determined on each image. The drop velocity is then obtained by differentiation of drop-centre coordinates on successive images. As the trajectory is vertical, only the vertical component $V_z$ will be presented and discussed.

We consider low-viscosity rising drops ($\rho_d/\rho_c = 0.69$, $\mu_d/\mu_c = 0.41$) of diameter $d = 2a$ ranging from 0.59 to 3.52 mm. In figure 2, the oscillation Reynolds number $Re_{osc}$ is plotted against the drop diameter, as well as the maximal values of the rise Reynolds number $Re_{asc}$ and the drop aspect ratio $\chi$ measured at the end of the recorded sequence. For diameters less than 1.30 mm ($Re_{asc} = 84$, $\chi = 1.011$) the terminal velocity is reached before the end of the sequence, while for larger diameters the drop is still accelerating. In any case, the average deformation is small ($\chi < 1.12$) and the oscillation velocity is large compared to the rise velocity ($Re_{osc}$ at least greater then $3Re_{asc}$), which leads us to expect that the oscillations of a clean drop can be well described by the theory derived without accounting for buoyancy.

Figure 3 shows the drag coefficient, $C_d = 4\Delta\rho g d/(3\rho_c V_z^2)$, against the rise Reynolds number. Experimental values are compared with the simulations for spherical drops at various viscosity ratios by Rivkind & Ryskin (1976) and Oliver & Chung (1987), and with the correlation for a rigid sphere by Schiller & Naumann (1933). The measured drag coefficients are far above the theoretical results for a clean drop of the same viscosity ratio. For $Re_{asc} \leqslant 84$ ($d \leqslant 1.3$ mm), experimental $C_d$ values of spherical drops that have reached their terminal velocity (see figure 4*a* for instance) are close to the theoretical results obtained for a rigid sphere. We can therefore conclude that the inner circulation within the drop is blocked by the Marangoni effect due to the presence of contaminants. For larger $Re_{asc}$, the experimental $C_d$ is even larger due to slight deformation and to the fact that terminal velocity has not been reached (figure 5*a*); there is nevertheless no doubt that contamination acts as well, since the departure from the expected $C_d$ value for a spherical clean drop is huge.

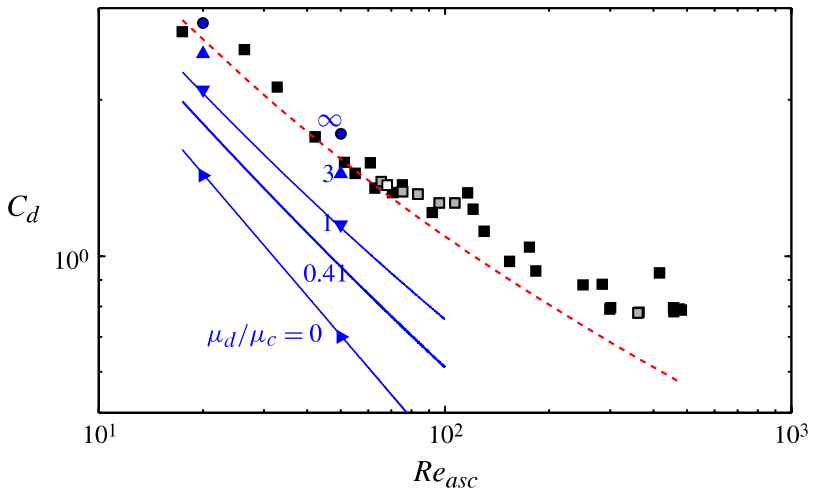


FIGURE 3. (Colour online) Drag coefficient against ascending Reynolds number. Squares, measurements (empty and grey symbols denote runs carried out after cleaning: see § 4 for details); (blue) circles and triangles, DNS by Oliver & Chung (1987) for a clean spherical drop of various viscosity ratios; solid (blue) lines, similar simulations by Rivkind & Ryskin (1976); dashed (red) line, correlation of Schiller & Naumann (1933) for a rigid sphere.

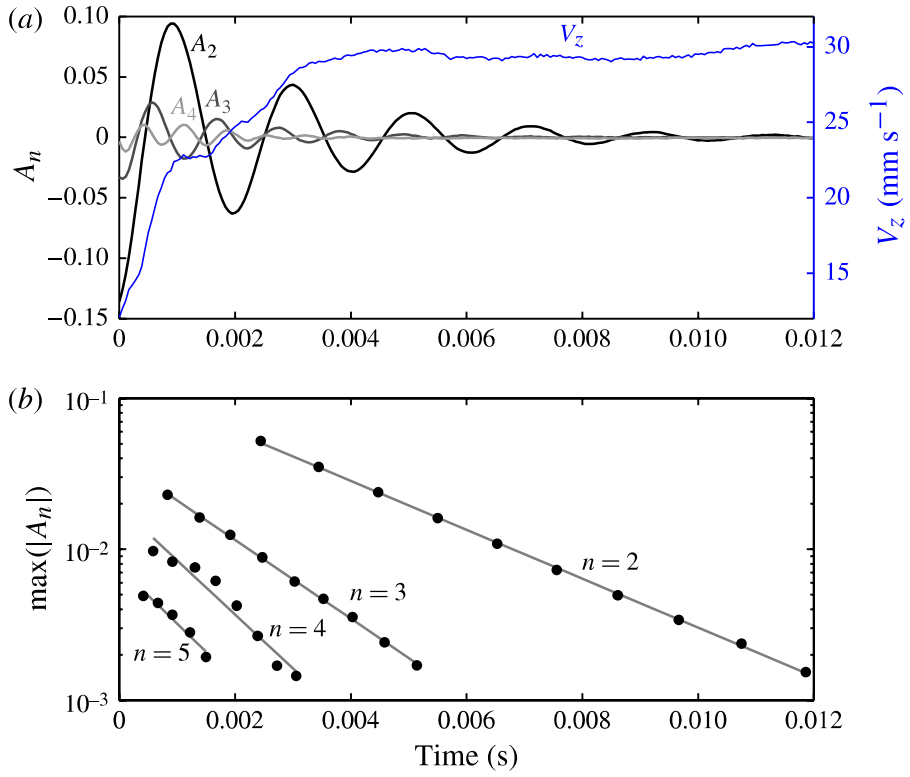


FIGURE 4. (Colour online) Time evolution of a drop of diameter $d = 0.59$ mm. (*a*) Amplitude $A_n$ of shape modes and rising velocity $V_z$. (*b*) Absolute values of the peak amplitude for each mode.

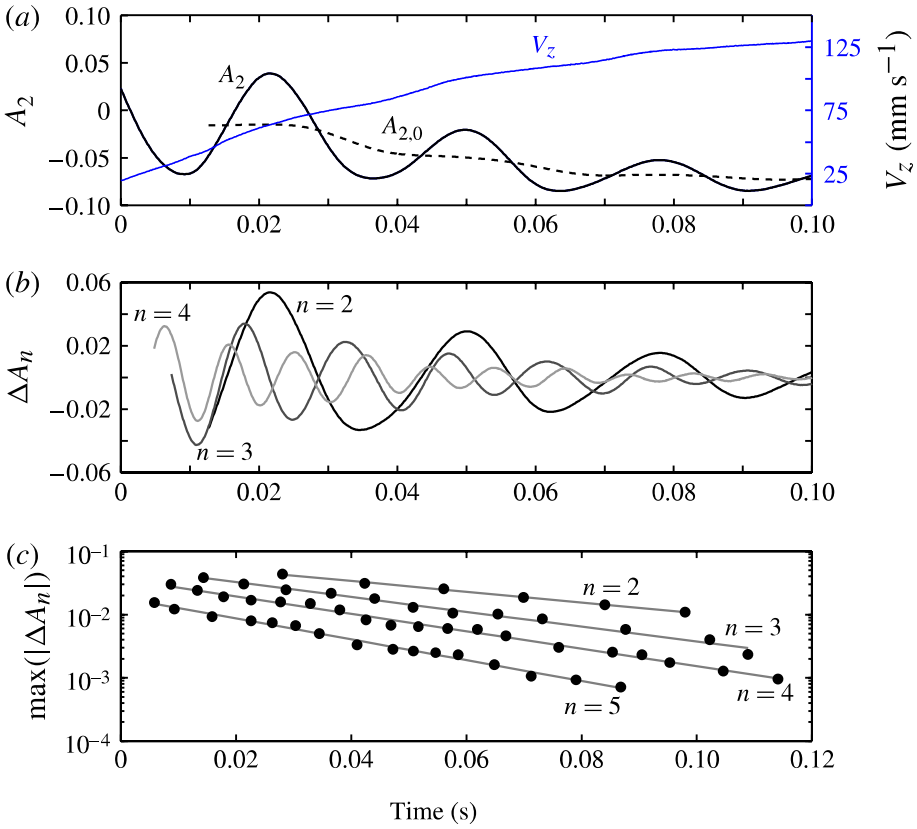


FIGURE 5. (Colour online) Time evolution of a drop of diameter $d = 3.52$ mm. ($a$) Total amplitude $A_2$ and slowly varying amplitude $A_{2,0}$ of mode two, drop rising velocity $V_z$. ($b$) Oscillation amplitude $\Delta A_n$. ($c$) Absolute values of the peaks of $\Delta A_n$.

## 3. Description of shape oscillations

As in ACRM, the drop contour is decomposed into spherical harmonics using spherical coordinates $(r, \theta)$ (figure 1):

$$r(\theta) = a\left(1 + \sum_{n=2}^{15} A_n(t) Y_{n,0}(\theta)\right). \tag{3.1}$$

The drop shape being axisymmetric, spherical harmonics reduce to Legendre polynomials, $Y_{n,0} = P_n(\cos(\theta))$. The series starts from $n = 2$ and stops at $n = 15$. The amplitude $A_0$ can be disregarded because of drop volume conservation. $A_1$ is zero since the origin of coordinates corresponds to the instantaneous drop centre position. Stopping the expansion at $n = 15$ was more than enough for an accurate description of the present drop shapes. The final accuracy in the determination of $A_n$ is better than $10^{-4}$ for $n \leqslant 5$.

Figure 4($a$) shows the time evolutions of the amplitude of the three first harmonics $A_2$, $A_3$ and $A_4$ as well as that of the drop centre velocity $V_z$ for the smallest drop ($2a = 0.59$ mm). A terminal velocity of 30 mm s$^{-1}$ is reached after approximately 6 ms. Amplitudes $A_n$ oscillate around zero, indicating that the mean drop shape remains spherical during ascension. The dominant harmonic $A_2$ exhibits damped oscillations at constant frequency. The amplitudes of secondary harmonics are dominated by their own frequency but are also slightly modulated by the frequency of $A_2$. Figure 5($a$) shows $V_z$ and $A_2$ for the largest drop ($d = 3.52$ mm). At the end of the recording ($t = 100$ ms), a terminal velocity of approximately 125 mm s$^{-1}$ is almost

reached but the oscillations are not yet totally damped out. The major difference with the smaller drop is that the drop shape around which oscillations take place is changing as the drop accelerates. The amplitude $A_n(t)$ of each harmonic is therefore the sum of a contribution $A_{n,0}(t)$ that slowly increases with time and a sinusoidal oscillation $\Delta A_n(t)$. $A_{n,0}(t)$ was determined by time-averaging over a moving window of duration equal to the period of oscillation. The oscillating part, $\Delta A_n(t)$, is illustrated in figure 5(*b*) for $n = 2$, 3 and 4. Compared to the smaller drop, harmonic 2 is less predominant and secondary harmonics are thus less influenced by harmonic 2.

In order to determine the decay of the oscillation modes, the absolute value of the successive minima and maxima of $\Delta A_n(t)$ were plotted against time in a semilog representation (figures 4*b* and 5*c*). For $n = 2$, all the measurements accurately lie on a straight line, indicating that the mechanical energy decays exponentially. For modes of higher order, a slight modulation is observed, caused by the fact that the corresponding oscillations occur on a shape that is mainly oscillating at mode 2. However, all the measurements are nicely distributed around straight lines for all modes and drop sizes. The slope of these straight lines corresponds to the damping rate $\beta_n$. A first important conclusion can be drawn: despite the fact that the drop velocity – and the shape of the largest drops – evolves with time, shape oscillations of rising drops exhibit constant angular frequency $\omega_n$ and damping rate $\beta_n$, as would be the case for clean and immobile drops.

## 4. Discussion of frequencies and damping rates

Based on the physical properties of the liquid phases, eigenfrequency $\omega_n^{th}$ of a clean non-rising drop is given by (1.2) with $B_2 = 0.534$, $B_3 = 0.740$, $B_4 = 0.945$ and $B_5 = 1.15$ (for general expressions of $B_n$ see (3)–(6) of ACRM: note that the last factor in the denominator of (5) should be squared). The presence of boundary layers at the interface hardly influences the eigenfrequencies that remain close to the potential theory prediction ($0.95 \leqslant \omega_n^{th}/\omega_n^* \leqslant 0.97$ for all $n$) and therefore scale as $d^{-3/2}$. Damping rate $\beta_n^{th}$ is given by (1.3) with $C_2 = 3.44$, $C_3 = 6.26$, $C_4 = 9.87$ and $C_5 = 14.3$ (for general expressions of $C_n$ see (4)–(6) of ACRM). It is controlled by the dissipation within the boundary layers. For all modes, the term proportional to the square root of the oscillation Reynolds number represents 79 % of $\beta_n^{th}$ for the smallest drop and 85 % for the largest one. Damping rate $\beta_n^{th}$ therefore scales as $d^{-7/4}$.

Figure 6 shows the frequency against the drop diameter for modes $n = 2$, 3, 4 and 5. The agreement between experimental values of $\omega_n$ (symbols) and $\omega_n^{th}$ (grey line) is remarkable for all modes and diameters. Whereas the rise velocity is drastically affected by interface contamination, oscillation frequencies of rising drops are close to that of a clean drop, as observed by ACRM for a drop attached to a capillary.

Figure 7 shows the damping rate against the drop diameter for modes $n = 2$, 3, 4 and 5. The symbols represent the measurements while the grey lines correspond to the theoretical prediction for a clean drop in the absence of gravity. Unlike the frequency, the experimental damping rates are much larger than the theoretical ones. The evolution of $\beta_n$ with the drop size is however parallel to that of $\beta_n^{th}$, approximately following a $d^{-7/4}$ power law, which indicates that the dissipation is still dominated by the boundary layers. The experimental damping rates are indeed well described by (1.3) provided that the theoretical prefactor $B_n$ of $\sqrt{Re_{osc,n}}$ is corrected by an empirical factor $K_n$: $B_n^{exp} = K_n \times B_n$ with $K_2 = 2.4$, $K_3 = 1.85$, $K_4 = 1.43$, $K_5 = 1.21$ (black lines in figure 7).

Suppression of interface contamination was attempted. All the equipment was cleaned with a degreasing agent (Eurostar 75N) and then carefully rinsed under

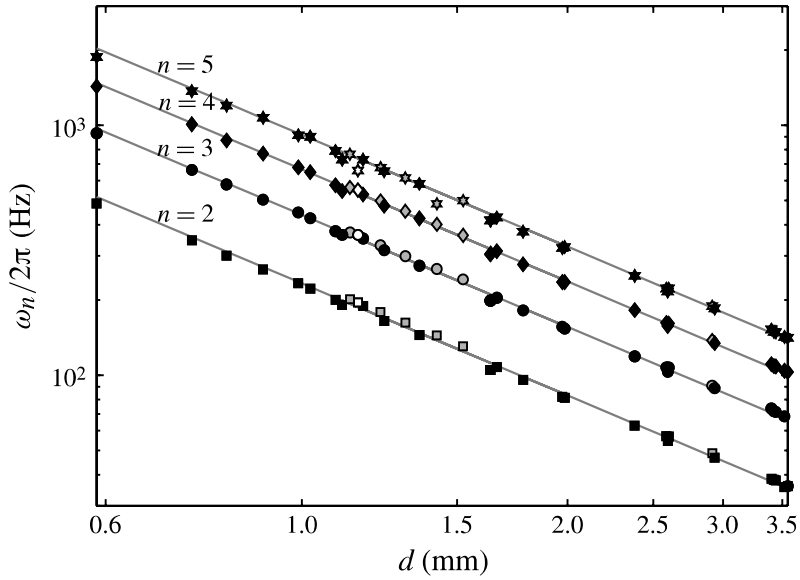


FIGURE 6. Oscillating frequencies against diameter for various modes. Symbols, measurements (empty and grey symbols denote runs carried out after cleaning); straight lines, the theoretical value (1.3) for a clean drop without considering gravity.

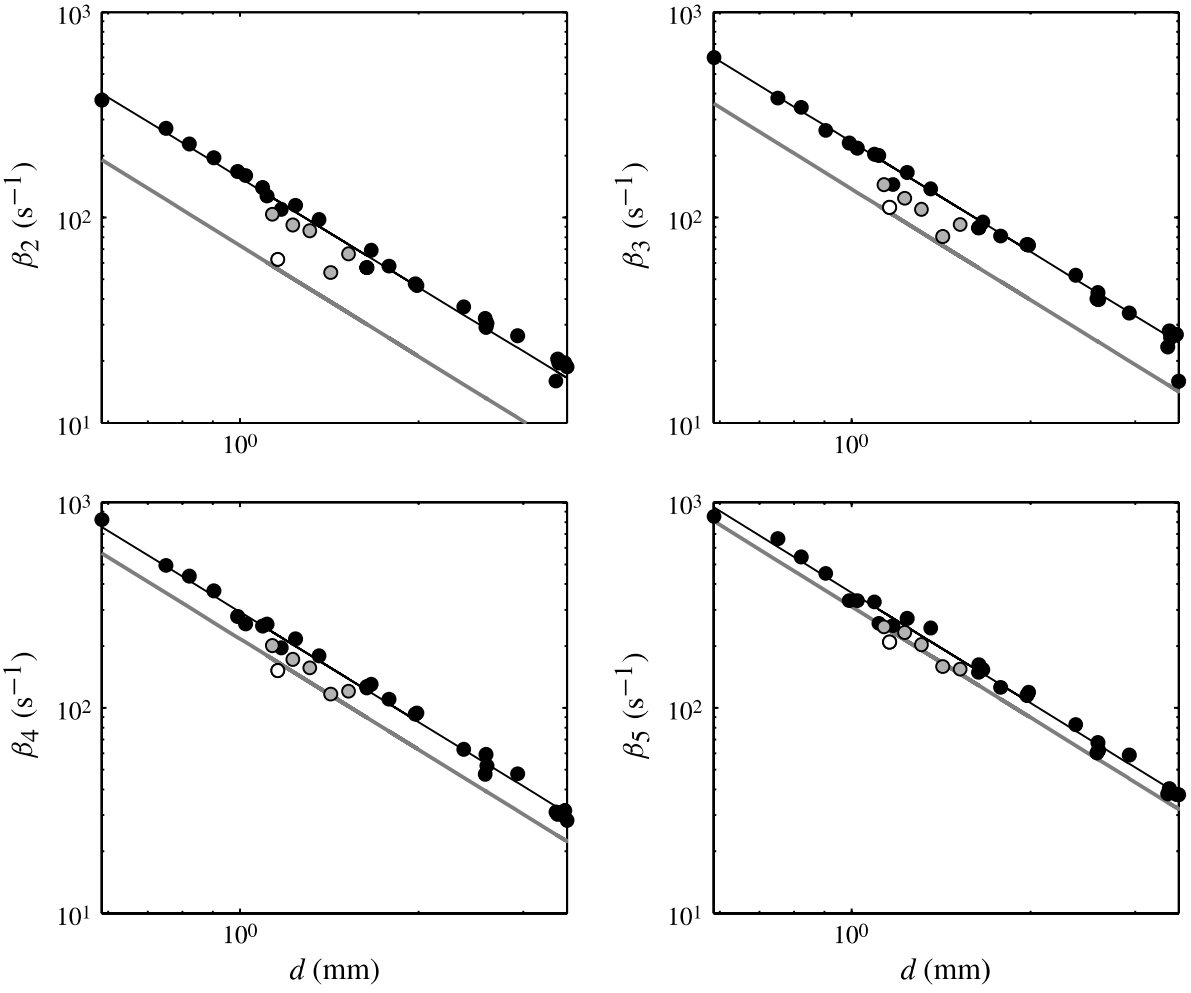


FIGURE 7. Damping rates against diameter for each mode. Symbols, measurements (empty and grey symbols denote runs carried out after cleaning); grey lines, the theoretical value (1.3) for a clean drop without considering gravity; black lines, (1.3) modified with $B_n^{exp}$.

flowing pure water; a new syringe was also used to inject heptane. A drop was released just after the cleaning. Its damping rate, represented by the empty symbol in figure 7, is indeed very close to $\beta_n^{th}$. Successive drops were thus released. Their damping rates (grey symbols) progressively move from the clean reference (grey line) towards contaminated values (black line). This suggests that the water–heptane interface, initially clean, becomes rapidly contaminated within the present experimental device, which is not suitable for work in ultra-clean conditions. Once the interface is sufficiently contaminated, measurements of damping rates are reproducible. Empty and grey symbols are used to represent drag coefficients and frequencies of these runs in figures 3 and 6 too. The corresponding values are not distinguishable from others. This was expected for $\omega_n$, since it is not affected by interface contamination, but it is rather surprising for $C_d$, which is considerably increased compared to that of a clean drop. As a matter of fact, the damping rate is less sensitive to surface contamination than the drag coefficient.

Let us turn back to fully contaminated damping rates (black symbols). ACRM observed that the damping rates of attached drops are not significantly affected by contamination. A minimum translation velocity $V_z$ is thus necessary for a Marangoni effect to develop so the contamination can alter the damping rates. Moreover, we observed that: (i) for a given run the damping rate remains constant as the drop accelerates; and (ii) for a given $n$ the value of $K_n$ is independent of the drop diameter. The present damping rates are thus independent of the drop velocity. Thus there should exist a threshold $V_{zc}$ above which the impact of the contamination on the damping rate saturates. The value of $V_{zc}$ is necessarily less than the velocity, $V_{zmin} = 15$ mm s$^{-1}$, attained by the smallest drop at the instant when the first values of the amplitude maximum are measured. The dimensionless group that controls this effect is the Péclet number, $Pe = 2aV_z/D_s$, where $D_s$ is the surface diffusion coefficient of the contaminants. Since $D_s$ is expected to be of the order of $10^{-9}$ m$^2$ s$^{-1}$ (Lu & Apfel 1991) and $2aV_{zmin} \approx 10^{-5}$ m$^2$ s$^{-1}$, the Péclet number is very large in all present experiments, which probably explains the independence of the damping rates on the rise velocity.

Another remarkable result is how the effect of the contamination on the damping rate varies with the mode number. The larger $n$, the smaller is $K_n$. This is probably related to the ratio between the wavelength, $\lambda_n = 2\pi a/n$, of the deformation and the length scale, $L_\sigma$, of the interfacial tension gradient along the interface. Since the Péclet number is large, the balance between advection and diffusion along the interface leads to $L_\sigma/\lambda_n \approx L_\sigma/2a = Pe^{-1} \ll 1$, where $\lambda_n$ is of the order of $2a$ at least for $n \leqslant 5$. The region where a significant gradient of interfacial tension exists and is able to cause an additional tangential stress within the oscillating boundary layer is therefore confined within a single wavelength of the shape oscillations. It is reasonable to think that affecting a single wavelength has less and less influence as the number $n$ of wavelengths increases.

Let us summarize the main findings. Inertial shape oscillations of a rising drop at small Weber number in a non-ultrapure environment have been investigated experimentally. As is commonly reported in the literature, the rise velocity is strongly affected by the presence of surface-active contaminants that are naturally present. The eigenfrequencies of shape oscillations are not affected by contamination. However, the damping rates are strongly increased, the effect being maximum for the largest wavelengths. Comparison with a fixed drop of the same fluids indicates that the rising motion is responsible for the increase of the damping rate. This phenomenon is therefore different from that reported for levitated drops (Lu & Apfel 1990) and is

probably related to an additional tangential stress within boundary layers at the drop surface caused by a Marangoni effect due to drop rising. It is also observed to be independent of the rising velocity, as a probable consequence of a large Péclet number. However, the boundary layers corresponding to drop translation and oscillation are different, and the damping rate turns out to be less sensitive to contamination than the drag coefficient.

## Acknowledgements

We thank C. Dalmazzone and C. Noik from IFP-Energies Nouvelles for fruitful discussions. The experimental setup was built with support of Czech Science Foundation (project no. P101/11/0806).

## REFERENCES

ABI CHEBEL, N., RISSO, F. & MASBERNAT, O. 2011 Inertial modes of a periodically forced buoyant drop attached to a capillary. *Phys. Fluids* **23**, 102104.

BASARAN, O. A., SCOTT, T. C. & BYERS, C. H. 1989 Drop oscillations in liquid–liquid systems. *AIChE* **35**, 1263–1270.

CUENOT, B., MAGNAUDET, J. & SPENNATO, B. 1997 Flow about a fluid sphere at low to moderate Reynolds numbers. *J. Fluid Mech.* **339**, 25–40.

DUINEVELD, P. C. 1995 The rise of an ellipsoidal bubble in water at high Reynolds number. *J. Fluid Mech.* **292**, 325–332.

HU, S. & KINTNER, R. C. 1955 The fall of single liquid drops through water. *AIChE* **1**, 42–48.

LU, H. & APFEL, R. E. 1990 Quadrupole oscillations of drops for studying interfacial properties. *J. Colloid Interface Sci.* **134**, 245–255.

LU, H. & APFEL, R. E. 1991 Shape oscillations of drops in the presence of surfactants. *J. Fluid Mech.* **222**, 351–368.

MILLER, C. A. & SCRIVEN, L. E. 1968 The oscillations of a fluid droplet immersed in another fluid. *J. Fluid Mech.* **32**, 417–435.

OLIVER, D. L. R. & CHUNG, J. N. 1987 Flow about a fluid sphere at low to moderate Reynolds numbers. *J. Fluid Mech.* **177**, 1–18.

PROSPERETTI, A. 1980 Normal mode analysis for the oscillations of a viscous liquid drop in an immiscible liquid. *J. Mécanique* **19**, 149–182.

RIVKIND, V. Y. & RYSKIN, G. M. 1976 Flow structure in motion of a spherical drop in a fluid medium at intermediate Reynolds numbers. *J. Fluid Dynam.* **11**, 5–12.

SCHILLER, L. & NAUMANN, A. Z. 1933 Über die grundlegenden Berechnungen bei der Schwerkraftaufbereitung. *Z. Vereines Deutscher Ingenieure* **77**, 318–320.

SUBRAMANYAM, S. V. 1969 A note on the damping and oscillations of a fluid drop moving in another fluid. *J. Fluid Mech.* **37**, 715–725.

VEJRAŽKA, J., FUJASOVA, M., STANOVSKY, P., RUZICKA, M. C. & DRAHOS, J. 2008 Bubbling controlled by needle movement. *Fluid Dyn. Res.* **40**, 521–533.

WEGENER, M., KRAUME, M. & PASCHEDAG, A. R. 2010 Terminal and transient drop rise velocity of single toluene droplets in water. *AIChE* **56**, 2–10.

ZENIT, R. & & MAGNAUDET, J. 2008 Path instability of rising spheroidal air bubbles: a shape-controlled process. *Phys. Fluids* **20**, 061702.